

Computational analysis *in vitro*: dynamics and plasticity of a neuro-robotic system

Amir Karniel¹, Michael Kositsky², Karen M Fleming²,
Michela Chiappalone³, Vittorio Sanguineti⁴, Simon T Alford⁵
and Ferdinando A Mussa-Ivaldi²

¹ Department of Biomedical Engineering, Ben Gurion University of the Negev, Beer-Sheva, Israel

² Department of Physiology, Northwestern University Medical School, Chicago, IL, USA

³ Neuroengineering and Bio-nanoTechnology Group (NBT), Department of Biophysical and Electronic Engineering—DIBE, University of Genova, Italy

⁴ Dipartimento di Informatica Sistemistica E Telematica, Università di Genova, Genova, Italy

⁵ Biological Sciences, University of Illinois at Chicago, Chicago, IL, USA

E-mail: sandro@northwestern.edu

Received 10 February 2005

Accepted for publication 5 July 2005

Published 31 August 2005

Online at stacks.iop.org/JNE/2/S250

Abstract

When the brain interacts with the environment it constantly adapts by representing the environment in a form that is called an internal model. The neurobiological basis for internal models is provided by the connectivity and the dynamical properties of neurons. Thus, the interactions between neural tissues and external devices provide a fundamental means for investigating the connectivity and dynamical properties of neural populations. We developed this idea, suggested in the 1980s by Valentino Braitenberg, for investigating and representing the dynamical behavior of neuronal populations in the brainstem of the lamprey. The brainstem was maintained *in vitro* and connected in a closed loop with two types of artificial device: (a) a simulated dynamical system and (b) a small mobile robot. In both cases, the device was controlled by recorded extracellular signals and its output was translated into electrical stimuli delivered to the neural system. The goal of the first study was to estimate the dynamical dimension of neural preparation in a single-input/single-output configuration. The dynamical dimension is the number of state variables that together with the applied input determine the output of a system. The results indicate that while this neural system has significant dynamical properties, its effective complexity, as established by the dynamical dimension, is rather moderate. In the second study, we considered a more specific situation, in which the same portion of the nervous system controls a robotic device in a two-input/two-output configuration. We fitted the input–output data from the neuro-robotic preparation to neural network models having different internal dynamics and we observed the generalization error of each model. Consistent with the first study, this second experiment showed that a simple recurrent dynamical model was able to capture the behavior of the hybrid system. This experimental and computational framework provides the means for investigating neural plasticity and internal representations in the context of brain–machine interfaces.

1. Introduction

Understanding and controlling neural dynamics and neural plasticity is a critical goal for developing effective interactions between the brain and artificial devices. In the last decades,

several experiments have directly addressed the ability of the nervous system to form internal models of the controlled dynamics (Bhushan and Shadmehr 1999, Gottlieb 1994, Inbar and Yafe 1976, Kawato 1999, Mussa-Ivaldi and Bizzi 2000, Wolpert *et al* 1995). A common element of these

studies is the establishment of a direct bidirectional interaction between the biological controller and an external system with programmable dynamics. Learning the dynamics of an external system is a fundamental challenge in the control of prosthetic devices and in the clinical application of brain machine interfaces (BMIs) which are an emergent technology with significant clinical potential (Donoghue 2002, Carmena *et al* 2003, Mussa-Ivaldi and Miller 2003, Musallam *et al* 2004). In recent studies, the information measured in the motor cortex of primates was used to guide robotic arms or to move computer cursors (Wessberg *et al* 2000, Serruya *et al* 2002). However, training the nervous system to control an artificial device is still a daunting task (Helms Tillery *et al* 2001, Taylor *et al* 2002).

In robotic systems, the adaptive representation of a controlled payload is typically implemented by lines of code in some programming language. The biological counterpart of such representation is assembled in our brains by modifiable (or ‘plastic’) patterns of neural connectivity and excitability. These patterns can be considered as the components of a biological programming language, whose rules are still largely unknown. Here we present two studies that used the interaction between a neural population and known external devices as a tool for investigating the rules of this language. In our studies, the neural component operates as a controller of the external device and the experiments are designed to identify specific properties of this biological controller. To this end, we established a bidirectional interaction between a neural population from the lamprey brainstem and an artificial device.

The lamprey nervous system has been extensively studied, particularly its ability to generate and modulate locomotor behavior (Grillner *et al* 2000). We have selected a portion of neural circuitry that integrates vestibular and other sensory signals and issues motor commands to stabilize the orientation of the body during swimming (Rovainen 1979, Deliagina 1997). This system has been shown to be adaptive: unilateral lesions of the vestibular capsules are followed by a slow reconfiguration of neuronal activities until the correct postural control is recovered (Deliagina 1997). Such adaptation is the first sign of an internal model, the second sign is the after effects of learning, a phenomenon that is observed when the perturbation is removed and an erroneous behavior is observed although the null conditions are reinstated (Shadmehr and Mussa-Ivaldi 1994). Unilateral lesion is an irreversible operation and therefore observing after effects is impossible. This is not the case for hybrid systems such as ours, where the sensitivity of the light sensors can be tuned out and then after adaptation tuned in again in order to observe the after effects of the adaptation.

In this paper we report two experiments, carried out on two different hybrid systems. In the first, we placed the lamprey brainstem in closed-loop interaction with simulated dynamical systems. The purpose of this experiment was to estimate, in rather general terms, the dimension of the state space in which one can describe the recorded activity of the neural preparation as a function of (a) an applied stimulation and (b) the past history of the same activity. We found that indeed the neural

tissue does not produce a mere algebraic map from input to output, but the current recorded activities depend upon earlier activities as well. However, the order of this dependency—i.e. the number of independent state variables necessary to predict the response to a given input—is rather limited. In practice, this suggests that it is possible to capture with relatively simple representations the dynamics of this neural element embedded in a closed loop interaction with an artificial dynamical system.

In the second experiment, we considered a more practical situation, in which the neural preparation interacted with a small mobile robot. Two stimulating electrodes carried information about light intensity detected by the robot sensors, and two extracellular recording electrodes detected the neural responses to these stimuli and provided the signal source that controlled the robot’s wheels. The nervous system between the four electrodes assumed the function of a controller—with two inputs and two outputs—that determined the behavior of the robot via a feedback loop. Unlike the first experiment, in the second experiment we considered specific parametric forms for the state/output equations characterizing the neural system. Here, we describe how this parametric representation—in the form of simple recurrent neural networks—allows us to capture not only the behavior of the hybrid system, but also some of the plastic changes induced by systematic alterations of the connectivity between the robot and the neural system.

2. Experiment 1: a closed-loop BMI for estimating neural dynamics

2.1. Basic paradigm and assumptions

The closed-loop interaction between a neural population and external devices can be exploited to extract some general dynamical properties of the neural population. Here, we describe recent studies (Kositsky *et al* 2003a, 2003b) in which we used the observed behaviors of this hybrid system to assess the *dynamical dimension* of the neurons in the lamprey’s reticular formation. The dynamical dimension (Abarbanel 1996) specifies how many independent state variables determine the output of a system at each instant.

In general mathematical terms (see figure 1), the artificial system connected to the neural tissue is described by the state and output equations:

$$\begin{cases} x_{t+1} = h(x_t, u_t) \\ y_{t+1} = p(x_{t+1}), \end{cases}$$

where x is the state of the external device, u is a control signal, y is the read-out signal, h and p are the functions, and the subscripts refer to discrete sampling time.

One can describe in the same way the neural preparation as a dynamical system. The main assumption of this study is that *there exists a state representation (s) of the neural preparation such that the changes of state are completely determined by the state itself and by the input to the neural preparation, i.e.:*

$$\begin{cases} s_{t+1} = f(s_t, i_t) \\ o_{t+1} = w(s_{t+1}). \end{cases}$$

Both s and x are vectors. In principle, there may be infinitely many equally valid representations for the state s .

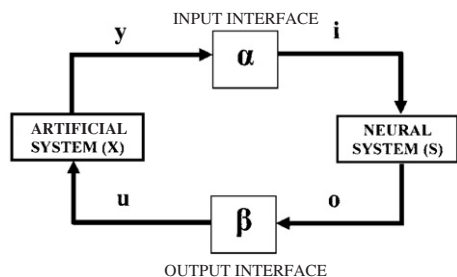


Figure 1. The brain–machine interface of experiment 1. The neural system and the simulated artificial system communicate via input and output interfaces. The input interface converts the output of the artificial system, y , into an electrical stimulus, i , which is the input of the neural system. The output of the neural system, o , is the recorded activity of a neuronal population. This activity is translated by the output interface into the control signal, u , driving the simulated artificial system. The artificial system has an (known) state vector, x , and the neural system has an (unknown) state vector, s . The combined hybrid system has a net state vector $q = [x, s]^T$.

However, its dimension (the dynamical dimension), that is the number of independent components in any complete numerical representation, is a fixed and well-defined property of the preparation, which we seek to determine.

The neural preparation and the external device are interconnected in a closed loop through two instantaneous mappings:

$$\begin{cases} i_t = \alpha(y_t) & \text{(input interface)} \\ u_t = \beta(o_t) & \text{(output interface).} \end{cases}$$

By combining these relations with the dynamics of both the external system and the neural preparation (i.e. the three equations above) one obtains a single differential equation:

$$q_{t+1} = m(q_t),$$

where $q = [x, s]^T$ is the state of the hybrid system and is a composition of the states of the two subsystems, the external device and the neural preparation, and

$$m = \begin{bmatrix} h(\cdot, \beta \circ w) \\ f(\cdot, \alpha \circ p) \end{bmatrix}.$$

Accordingly,

$$\dim(q) = \dim(x) + \dim(s).$$

This equation does not hold true in the general case. A more rigorous formulation leads to the inequality:

$$\dim(q) - \dim(x) \leq \dim(s) \leq \dim(q).$$

This can be seen by observing that the dimension of the hybrid system cannot exceed the dimension of each component. Therefore,

$$\dim(q) \leq \dim(x) + \dim(s).$$

However, since we analyze obtained data using real neural preparations, it is improbable that the neural component and the external system would combine into a system of lower dimension as in the inequality above. It is obvious that the hybrid system dimension is likely to be an upper bound for the neural component dimension:

$$\dim(s) \leq \dim(q).$$

This last inequality is readily proven for linear systems by considering that the rank of the hybrid system’s state transition matrix cannot be lower than the rank of either subsystem.

By construction, the behavior of the hybrid system does not depend on any external input, but only on its current state: this is the defining property of an ‘autonomous system’. In any practical case, autonomy is only an approximation, as uncontrolled external inputs cannot entirely be discounted. However, we assumed that these external inputs may be neglected. We assessed the dynamical dimension of the hybrid system, $\dim(q)$, by collecting multiple trajectories of the external device. Then, we computed the dynamical dimension of the neural preparation by subtracting the known dimension of the external system from the estimated dimension of the combined system:

$$\dim(s) = \dim(q) - \dim(x).$$

The main element of novelty with this approach stems from the possibility of using external systems with different dimensions. Then, one can use the known difference between the dimensions of the external systems as a condition to validate the stability of the neural dimension estimate.

We need to stress that particular caution is required when dealing with nonlinear dynamics, as in such cases the dimension estimated by local embedding methods may be smaller than the actual dimension of the system over the entire state space.

2.2. Neural preparation

The neural component of the hybrid system was a portion of the brainstem of the sea lamprey (*Petromyzon marinus*) in its larval state. After anesthetizing the larvae with tricaine methanesulphonate, the whole brain was dissected and maintained in continuously superfused, oxygenated and refrigerated Ringer’s solution (details in Alford *et al* (1995)).

We chose to use the vestibular–reticulospinal synapse because (a) it is relatively well understood in its anatomy and physiology; (b) it allows accessing neuronal populations under visual guidance; and (c) the whole brain can easily be maintained *in vitro* by immersion in a refrigerated Ringer’s solution.

We recorded extracellularly the activity of neurons in a region of the reticular formation, a relay that connects different sensory systems (visual, vestibular and tactile) and central commands to the motor centers of the spinal cord. We placed a recording electrode in the axons of the posterior rhombencephalic reticular nucleus (PRRN). We also placed a unipolar tungsten stimulation electrode among the axons of the posterior octavomotor nucleus (nOMP). The stimulating electrode was placed on the side of the midline opposite to the recording electrode. nOMP receives inputs from the vestibular capsule and its axons form synapses with the rhombencephalic neurons on the opposite side of the midline (see figure 5, top left).

We placed the stimulating electrode near the nOMP, thus stimulating a large proportion of fibers that crossed the midline. This induced predominantly excitatory responses in the downstream neurons. The recorded signals were acquired

Table 1. The spike detection procedure used in experiment 1.

loop along values of the acquired signal, $r(t)$, where t is time
 find the next local maximum, $r(t_i)$, such that $r(t_i) > r(t_{i-1})$,
 $r(t_i) > r(t_{i+1})$
 find the next local minimum, $r(t_j)$, such that $j > i$, $r(t_j) < r(t_{j-1})$,
 $r(t_j) < r(t_{j+1})$
if $r(t_i) - r(t_j) > \text{min spike magnitude}$ **and** $t_j - t_i < \text{max spike}$
 duration assign spike at time t_i

at 10 kHz by a data acquisition board (National Instruments PCI-MIO-16E4).

The procedure used for online spike detection in this experiment is described in table 1. The minimal spike magnitude and the maximal spike duration parameters were set to 1.1 mV and 1 ms respectively. To avoid confusion between stimulation artifacts and spikes, the acquired raw signal immediately following each stimulation pulse was discarded. The duration of discarded signal (the artifact cancellation period) was set to 3 ms. The spike detection procedure in table 1 skips segments of the raw signal during the artifact cancellation periods.

2.3. Artificial systems

We used two different artificial systems with dynamical dimensions of two and four. These systems simulated in real time were, respectively, a single point-mass and two masses connected in series by a spring. The masses were free to move along a line. For both systems, the control signal u determined the external force acting on one mass, whose position was the read-out signal y . A critical goal in this type of study is to explore a sufficiently large variety of behaviors, so that the observed states may cover a sufficiently large region. To this end, nonlinearities and dissipation were added to the external system: the point-masses were constrained to move within a (nonlinear) potential field, and a damping element was introduced between each point-mass and the ground.

2.4. Procedure

An experimental session consisted of a sequence of 20 episodes, each lasting 20 s. While the neural signal was sampled at a rate of 10 kHz, the external system simulation and the interfaces between the neural and external components were run at a rate of 20 Hz. The two external systems were used in alternating episodes. For each episode, the initial configuration of the corresponding external system (positions and velocities of the point-masses) was drawn at random. As expected, the trajectories of the external device had multiple self-intersections. Sample trajectories of the external devices used for the further analysis are shown in figure 2. The trajectories provide a visual cue of possible chaotic dynamics. The observed trajectories, y_t , were one-dimensional projections from a higher dimensional state space, where the state trajectories of an autonomous system do not intersect themselves or each other (Arnold 1978).

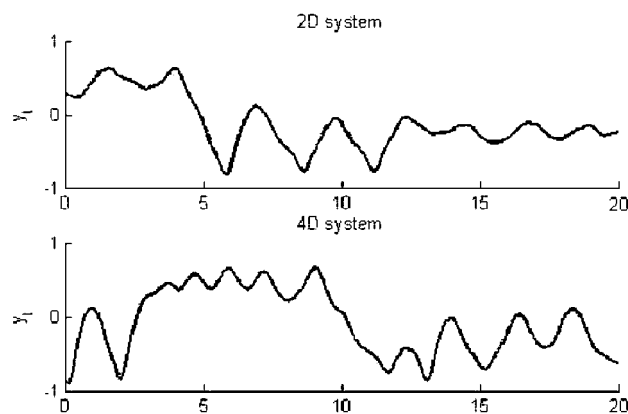


Figure 2. Sample trajectories of the external dynamical systems. The upper panel shows a trajectory obtained using the 2D system, the lower panel shows a trajectory obtained using the 4D system. These trajectories were obtained using preparation 1.

2.5. Dimension analysis

To reconstruct the proper dimension of the hybrid system's state space, we unfolded the observed trajectories into spaces of increasing dimensions and estimated the presence of intersections (Kaplan 1994). The lowest dimension where the trajectories did not intersect was judged to be an adequate estimate of the dynamical dimension of the hybrid system (Abarbanel 1996, Kaplan 1993).

To unfold trajectories into a space of a given dimension d , we used the delayed coordinate space embedding (Takens 1981, Mane 1981), consisting of d consecutive values of the original trajectory:

$$v_i = (y_i, y_{i+\tau}, \dots, y_{i+(d-1)\tau}),$$

where i enumerates the state-points along the embedded state trajectory and τ is an integer lag parameter. To select a proper lag τ , we have employed an approach that uses the first (corresponding to the smallest τ) local minimum of the mutual information between samples (Abarbanel 1996). Estimating the presence of trajectory intersections is a difficult and somewhat controversial task (Ruelle 1990). Trajectories are sets of measure zero within the embedding space, and one can never observe an actual intersection. In spaces of dimension larger than two, it is only possible to determine that two trajectory segments are close to each other. Most of the existing methods for dimension reconstruction address this difficulty (Kaplan and Glass 1992, Kennel *et al* 1992).

We used the 'delta-epsilon method' developed by Kaplan (1994) (figure 3).

For each dimension d , the trajectories were unfolded in d -dimensional space and pairs of consecutive points along the unfolded trajectories were analyzed. For two pairs (v_i, v_{i+1}) and (v_j, v_{j+1}) , the distance between the first points of each pair is denoted by δ : $\delta = |v_i - v_j|$, and the distance between the second points of each pair is denoted by ϵ : $\epsilon = |v_{i+1} - v_{j+1}|$. Delta-epsilon combinations with small deltas (approaching the limit $\delta \rightarrow 0$) and large epsilons are interpreted as intersections of the trajectories due to projection from a higher dimensional state space onto a space of insufficient dimension.

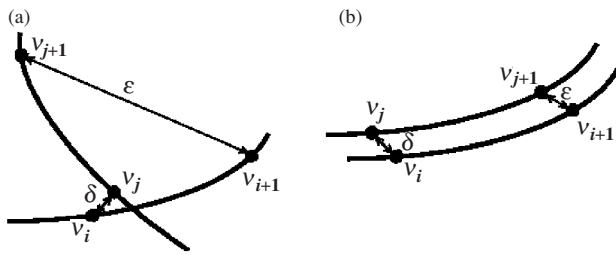


Figure 3. Kaplan's δ - ϵ analysis (Kaplan 1994). Consider pairs of points, (v_i, v_j) , and their successors along corresponding trajectories, (v_{i+1}, v_{j+1}) . Let $\delta = |v_i - v_j|$, $\epsilon = |v_{i+1} - v_{j+1}|$. (a) When small δ bear large ϵ , it is interpreted as intersecting trajectories. (b) If trajectories do not intersect, small δ always bear small ϵ .

If small deltas always bear small epsilons, this is interpreted as an indication that $\delta \rightarrow 0$ implies $\epsilon \rightarrow 0$ corresponding to the elimination of all intersections of the trajectories. In this case, the embedding dimension (d) is deemed to be an adequate estimate for the dimension of the state space. For each dimension, we computed the delta-epsilon combinations and considered n combinations with the smallest deltas. To test for trajectory intersections in a given dimension d , we compared the magnitudes

$$\epsilon_d = \max_{(\delta, \epsilon) \in Z_n} \epsilon$$

for different d . Z_n is the set of n delta-epsilon combinations with smallest deltas. As the dimension d increases, ϵ_d decrease almost monotonically until they reach a plateau. This saturation points to the dynamical dimension of the hybrid system d_* .

To address the problem of noise in the dimension analysis, ten surrogate trajectories were generated for each original trajectory using randomized phases. These trajectories do not reflect any implicit dependencies and are used as examples of 'pure noise'. Any dimension estimate applied to these trajectories should tend to infinity.

2.6. The dynamic dimension of the neural preparation

The results of the delta-epsilon analysis with the two external devices are shown in figure 4 together with the results of the analysis of the surrogate trajectories. The latter results stand in agreement with the assumption that noise has infinite dynamical dimension. They serve as a good reference baseline for assessing decay and saturation in the original trajectories. To address the arbitrariness in the parameter choice, which might affect the results, we used, among other factors, the consistency between the results for the 2D and the 4D external systems: the difference between the corresponding dynamical dimensions is equal to 2. For preparations 1 and 2 (figures 4(a) and (b)), the estimated dynamical dimension of the hybrid system, d_* , was 4, with the 2D external system, and 6, with the 4D external system. Thus, the estimated dynamical dimension of the neural component for these preparations was equal to 2. For preparation 3, (figure 4(c)), d_* was equal to 5, with the 2D external system, and to 7, with the 4D external system. Thus,

the estimated dynamical dimension of the neural component for preparation 3 was equal to 3.

The obtained low dimension estimates indicate that the neural dynamics can be captured by relatively simple descriptive models, consistent with the parametric analysis discussed below. Here, one must take into account that the analysis refers to population signals detected by a single extracellular electrode and should not be extrapolated to represent the detailed dynamical behavior of individual neurons. Nevertheless, the observation of low-order dynamics in this constrained experimental context provides critical support for the study of experiment 2, where the neural population behavior is represented by a low-order parametric model.

3. Experiment 2: recurrent dynamics in a neuro-robotic system

The system used for this study included three elements: a neural preparation, a robot and an interface (figure 5).

3.1. Neural preparation

The neural component of the hybrid system was the same as in experiment 1. The vestibular-reticulospinal synapses of lampreys have well-documented plastic properties. High-frequency stimulation of the presynaptic zones leads to LTP (Alford *et al* 1995) while low-frequency stimulation leads to LTD. In addition Deliagina and colleagues have demonstrated that lesions of the pathway in the otherwise intact lamprey lead to long-term adaptive changes (Deliagina 1997).

In experiment 2, we used two pairs of stimulation and recording electrodes, one on each side of the midline (figure 5). The stimulating electrodes were placed at a site where the axons from nOMI and nOMP cross each other. Therefore, the stimulation on each side generated a bilateral response in the PRRN. To verify the placement of the stimulating electrodes we delivered brief single stimulus pulses (200 μ s) and observed the response in both the ipsi- and contralateral PRRN neurons. Once we determined that the stimulating electrodes were properly placed, we moved the recording electrodes caudally, in order to pick up population spikes. In some experiments, the stimulation had a biphasic (negative current followed by a positive current) rather than a monophasic (negative current only) waveform, to induce less charge buildup and less redox reaction at the stimulating electrode surface. This allowed us to extend the stability of the preparation and to reduce the likelihood of tissue damage during the barrage of stimuli caused by 'sensing' and moving in the robot.

The spiking activities of the PRRN as recorded near the axons were analyzed through a five step process (see also figure 5). The signal picked up by the recording electrodes contained a combination of spikes, stimulus artifacts, and other components that we considered as noise. To suppress slow components, the signal was first put through a high pass filter (cutoff at 200 Hz). The output of this filter contained high-frequency noise, stimulus artifacts, and the spikes generated

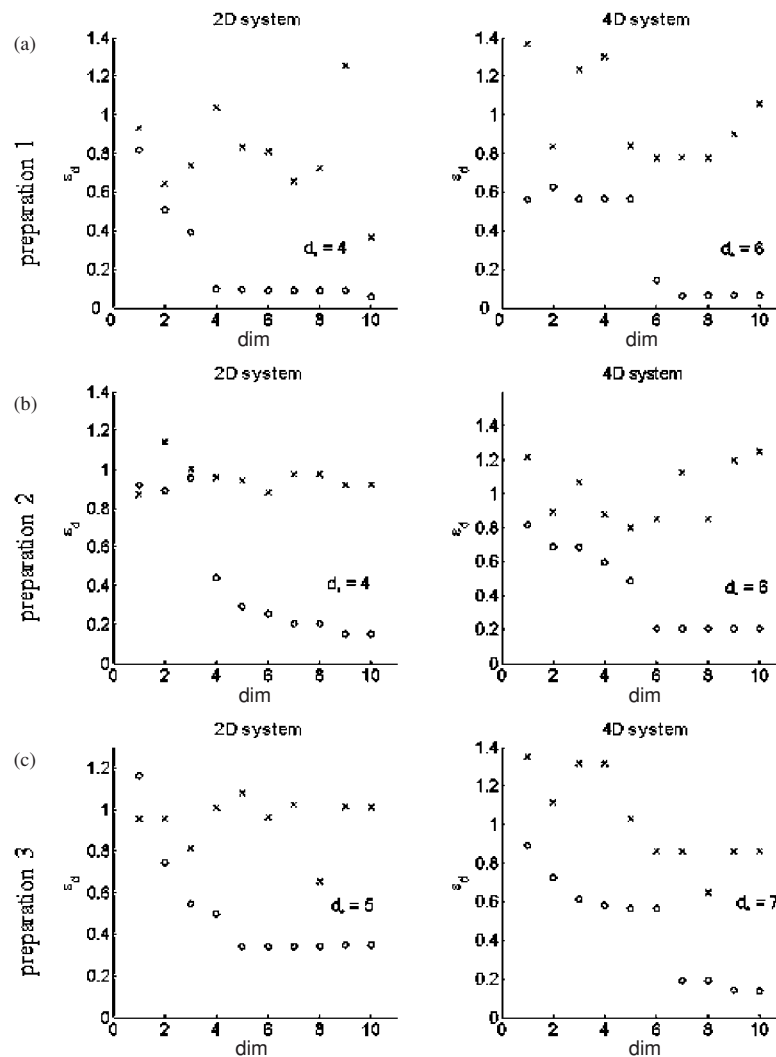


Figure 4. ε_d as a function of d (see the methods in section 2.5). As the dimension d increases, the corresponding magnitudes ε_d decrease almost monotonically until they reach a plateau, which points to the dynamical dimension of the hybrid system d_* . For each preparation, the left panel shows the data collected using the 2D external dynamical system, the right panel shows the data collected using the 4D external dynamical system. The Xs show ε_d computed for surrogate trajectories obtained by randomizing phases of the original trajectories. For preparations 1 and 2, the dynamical dimension of the hybrid system, d_* , is equal to 4, when the 2D external system is used, and to 6, when the 4D external system is used. The estimated dynamical dimension of the neural component for preparations 1 and 2 is equal to 2. For preparation 3, d_* is equal to 5, when the 2D external system is used, and to 7, when the 4D external system is used. The estimated dynamical dimension of the neural component for preparation 3 is equal to 3.

by multiple neurons in the vicinity of the electrode. Stimulus artifacts were canceled by zeroing the recorded signals over temporal windows of 4 ms following the delivery of each 200 μ s stimulation pulse. The remaining signal was rectified, and a threshold was applied to separate the spikes from the background noise—under the assumption that the spike amplitude was much larger than the noise amplitude. The resulting train of spikes was put through a low-pass filter (5 Hz), which effectively generated a rate coded signal. The mean of this signal over 300 ms provided a velocity control signal for each of the robot's wheels. As an additional test of the ability to detect the presence of active neural processes, as distinct from background noise and passive conduction of the stimulus artifacts, we verified that the interface did not generate any artifactual response when the recording electrodes were

placed in a passive medium such as Ringer's solution and dead tissue. The bottom plate in figure 5 demonstrates the recorded signal and the spike detection.

3.2. The robot and its workspace

The robot system was the base Khepera module (K team). Its workspace was a circular region with 2 ft diameter (figure 6). Eight sensors along the circumference of the robot provided proximity and light intensity information. The sensors were located on opposite sides of the robot's midline at 10°, 45°, 85° and 165° from the front position. Two wheels provided a means of locomotion. The computer system communicated with the robot through the serial port and a custom designed LabVIEW® application. Eight computer-controlled lights

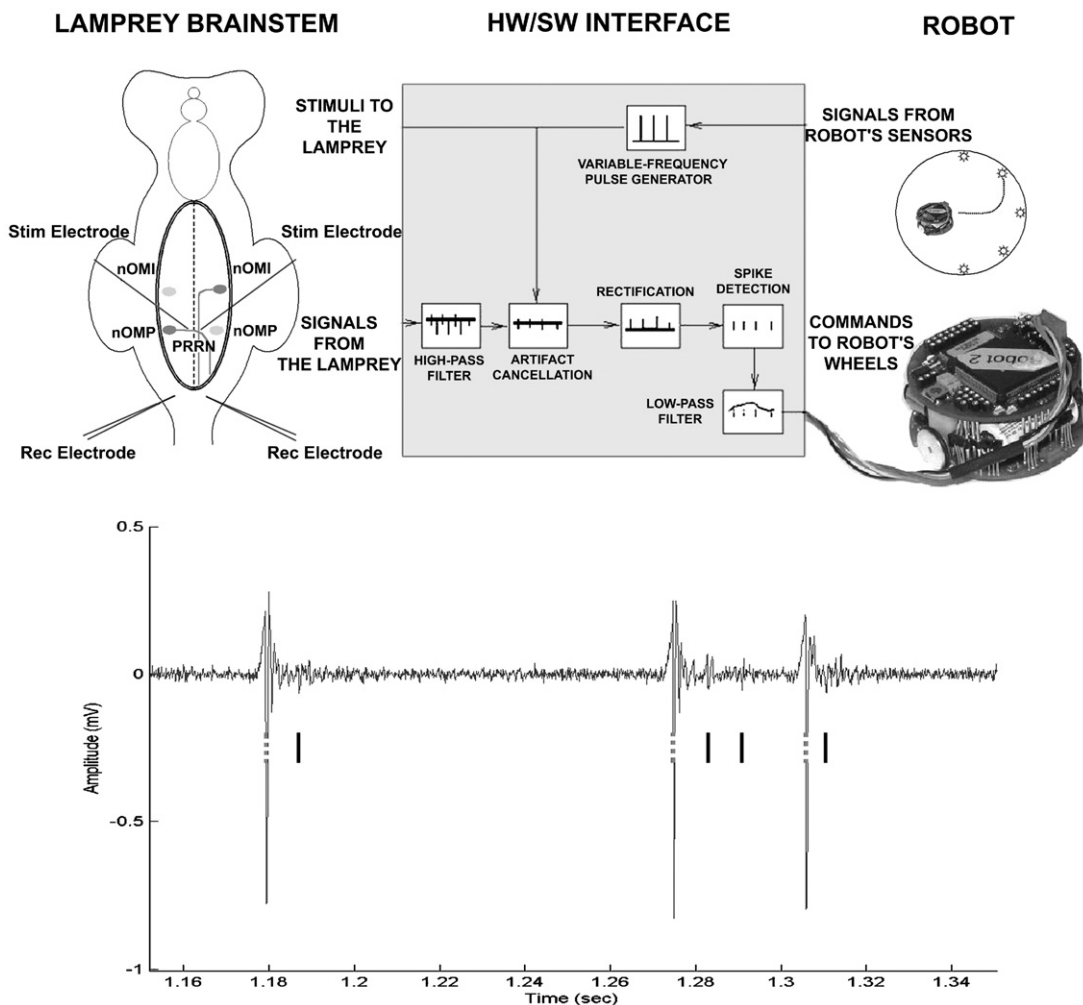


Figure 5. The hybrid system of experiment 2. A sketch of the neural preparation and the electrodes placement (top left). The two-wheeled robot (Khepera module, top right). The interface (top middle) between the robot (right) and the lamprey preparation (left) implemented in LabVIEW[®]. The two inputs and two outputs (right and left) are processed separately except for the artifact cancellation that influences both output channels right after the generation of stimulus in one of the channels. The trace in the bottom of the figure demonstrates recorded signal detected spikes (solid marks) and detected stimulus artifacts (dashed marks).

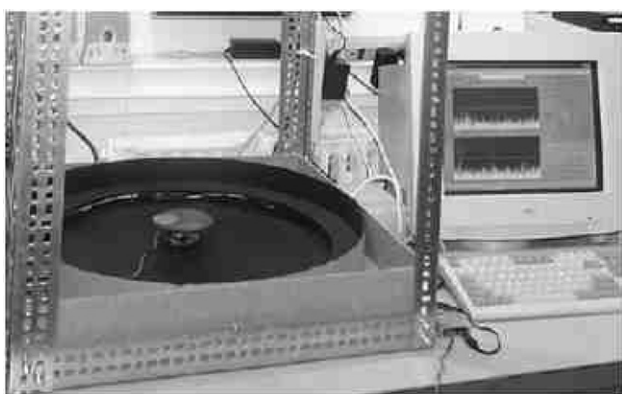


Figure 6. The robot in the workspace.

were mounted at the edge of the workspace at 45° intervals. These lights generated the stimuli that elicited the phototactic responses.

3.3. The interface

As in experiment 1, the interface acted as an interpreter between neural signals and the robot control system. It was responsible for transforming the robot's light sensor information into electrical stimuli and for processing in real time the neural activity of the reticulospinal nuclei and translating it into motor commands for the robot.

The light intensity detected by the robot sensors determined the frequencies at which the right and left vestibular pathways were stimulated. We multiplied the sensor outputs by weighting coefficients, which gave the greatest strength to sources of light at 45° and suppressed the rear sensors. The weighted sum of the sensors on each side was multiplied by a gain factor, which determined the maximum stimulation frequency. The final outcome of these operations was the frequency at which we stimulated each side. We used the digital counter on the acquisition board to generate a

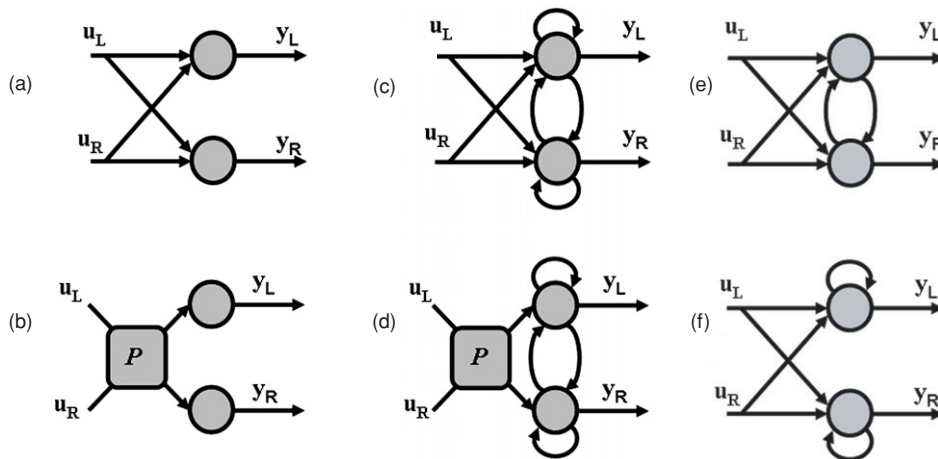


Figure 7. Models for lamprey brainstem neurons. (a) Static linear model. (b) Static polynomial model. (c) Dynamic linear model. (d) Dynamic model with polynomial input function. (e) Dynamic linear model without ipsilateral dynamic connections. (f) Dynamic linear model without contralateral dynamic connections.

pulse train, which was delivered to the neural preparation after passing through ISO-Flex stimulus isolators.

3.4. Interface calibration

The interface was calibrated so as to compensate for random differences between the recorded responses from the left and right side of the brainstem. Indeed, the net intensity of the signal picked up by each electrode was affected by a number of uncontrollable factors, such as the actual distance from signal sources. To compensate for these random factors, we made the working assumption that when both left and right sides are stimulated at the same frequency, the same motor response should be obtained on each side of the robot. This corresponds to considering all initial asymmetries between right and left sides as accidental features of no significance. Accordingly, all initial differences between right and left responses to the same right and left signals were balanced by regulating two output gains.

The connectivity between recording electrodes and robot wheels was either ‘direct’ or ‘reverse’. In the direct mode, the electrode on each side was connected via the interface to the wheel of the same side (right to right and left to left). In the reverse mode, the electrode on each side was connected to the wheel on the opposite side. The mode was established at the beginning of each experiment based on the initial response of the robot to a light source. If the response was a positive phototaxis (overall movement toward the light source) the direct mode was chosen. Otherwise, the reverse mode was chosen. This insured that positive phototaxis was always the prevalent behavior. The purpose of this procedure was to avoid negative phototaxis, because as the robot moved away from the light source, the intensity detected by the sensors tended to drop sharply. As a consequence, the trajectories were very short. Switching to the reverse configuration was sufficient to ensure an extended response in these cases. We have analyzed the data of each group separately but did not observe any

significant difference and therefore we report the results of both groups together.

3.5. Neuronal models and simulations

For each individual experiment, we obtained a model of the empirical input/output transformation for the left and right PRRN by fitting a bivariate function to the light sensor data (stimulus/input) and wheel motor commands (response/output). Next, we describe the various models that were considered and the data for the fitting and testing procedure.

Each model is a two-inputs/two-outputs system. Let u_L and u_R indicate light intensity transformed into the frequencies of the stimuli delivered by the left and right electrodes and let y_L and y_R indicate the firing rates recorded in response to these stimuli from the right and left PRRNs transformed into wheel speeds directed to the robot’s wheels. Then, a simple linear-static model for the lamprey’s brain is (see figure 7(a)):

$$\begin{aligned} y_L(n) &= w_{LL}u_L(n-1) + w_{LR}u_R(n-1) \\ y_R(n) &= w_{RL}u_L(n-1) + w_{RR}u_R(n-1). \end{aligned}$$

The parameters, w_{ij} , were determined by least-squares approximation of the input/output data and form collectively a 2×2 matrix W . The elements of W can be considered as connection weights between vestibular axons and reticular neurons. Positive weights represent excitatory connections and negative weights represent inhibitory connections. This simple linear static model (figure 7(a)) generates various behaviors, such as moving towards a light, away from the light or circling a light source (see Braitenberg (1984)). We used this model as a reference and compared the performances of other more complex models with its performance. For each lamprey and in each condition, the data of one set of trajectories (test set) were not used for estimating the parameters. The parameters that best approximated the rest of the data (fitting set) were used to predict the network output over this test set. This procedure was repeated for each set of trajectories

in order to achieve a good estimate of both fitting and testing (i.e., generalization) errors.

We also considered nonlinear functions of the inputs,

$$\begin{aligned} y_L(n) &= P_L\{u_L(n-1), u_R(n-1)\} \\ y_R(n) &= P_R\{u_L(n-1), u_R(n-1)\} \end{aligned}$$

where $P_{L,R}$ are polynomial functions. For example a second-order polynomial model took the following form:

$$\begin{aligned} y_L(n) &= a_{L1}u_L(n-1) + a_{L2}u_R(n-1) + a_{L3}u_L^2(n-1) \\ &\quad + a_{L4}u_R^2(n-1) + a_{L5}u_L(n-1)u_R(n-1) \\ y_R(n) &= a_{R1}u_L(n-1) + a_{R2}u_R(n-1) + a_{R3}u_L^2(n-1) \\ &\quad + a_{R4}u_R^2(n-1) + a_{R5}u_L(n-1)u_R(n-1). \end{aligned}$$

In this study, we considered polynomials of up to the fourth degree. The number of parameters increased with polynomial degree as follows: second degree, 10 parameters; third degree, 18 parameters; fourth degree, 28 parameters.

We also explored the additional explanatory power of linear dynamic models, i.e., models that take into account the previous neuronal activity and therefore represent recurrent loops and/or memory dependence in the time scale of seconds. The first-order dynamic model was the following (see figure 7(c))

$$\begin{aligned} y_L(n) &= w_{LL}u_L(n-1) + w_{LR}u_R(n-1) \\ &\quad + v_{LL}y_L(n-1) + v_{LR}y_R(n-1) \\ y_R(n) &= w_{RL}u_L(n-1) + w_{RR}u_R(n-1) \\ &\quad + v_{RL}y_L(n-1) + v_{RR}y_R(n-1). \end{aligned}$$

We then considered polynomial input functions as described above with the dynamic model, and finally, since the first-order dynamic model was found to be most appropriate, we also explored the role of ipsilateral and contralateral connections by considering two models that included only one type of these connections (see figures 7(e) and (f)). Altogether we have considered four static models, and six dynamic models. All the above models are in effect special cases of the Volterra series, which is an infinite polynomial moving average time series (see Barahona and Poon (1996)).

3.6. The data for fitting and testing

The basic set of data is a single trajectory of the robot that starts to move from the center of the workspace in response to a light that is turned on. We used the values of inputs and outputs measured and generated at the time steps of the control loop (twice in each second). Each of the five lights was turned on—one after the other—with a short break for returning the robot to the initial position. Each trajectory lasted about 5–10 s and typically contained more than ten sampling points. In each condition (before and after adaptation/control protocol), a few sets of five trajectories were recorded (typically four sets). We took one set out and fitted each of the models to the rest of the data. The residual of this fitting yielded the fitting mean-square error (MSE). The estimated parameters were used to predict the output in the generalization set. This prediction compared with the actual data yielded the testing MSE. In order to better estimate the fitting and testing errors, we have repeated the procedure where each time we took

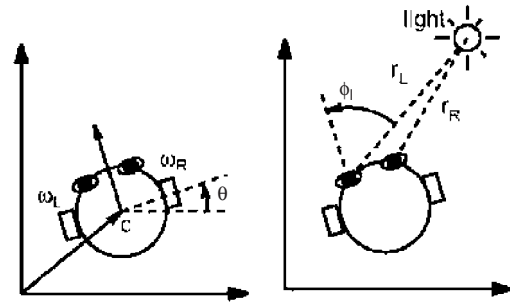


Figure 8. Robot's sensory motor system simulation. Left: motor system, the change in the position is a function of the current position and the velocity of the wheels. Right: sensory system, the light intensity perceived at each side of the robot is a function of the robot position and the light position.

out another set of data. We did this exhaustively, therefore if there were n sets of trajectories, we have repeated it n times each time fitting $5(n-1)$ trajectories to each model and then testing on the five trajectories that were not used for the fitting. The means over the n sets of each error (fitting and testing) were calculated and are referred to as learning error and generalization error for that condition and for that specific model. Then, the means over preparations and over different conditions were also calculated. The bootstrapping method of choosing every possible combination was used to gain an accurate estimation of the actual MSE for the learning and generalization in each condition. In order to calculate confidence intervals we used standard methods that employ the MSE for each condition only once, i.e., when performing a statistical test to compare two or more models, the number of data points was equal to the number of preparations where the MSE for each data point was the mean of testing or fitting errors as described above. For further details about cross validation and the problem of over-fitting, see, e.g., Haykin (1999), Karniel and Inbar (2000).

We report the results of fitting of ten models to the data gathered from 31 preparations before and after adaptation/control experiments. Therefore, 620 values of learning errors and the same number of generalization errors were the output of this data analysis.

3.7. Simulation of the whole hybrid system

In order to compare the capabilities of the neuronal models we have conducted simulation of the whole system. These simulations combined a discrete neural model (figure 7) with a continuous model for the robot and the sensors (figure 8).

For the continuous model, the state variables were the position and orientation of the robot. The following first-order nonlinear system was deemed to be adequate to capture the robot's behavior, since the control signal dictates the velocity of the wheels and the mass of the robot is negligible (see figure 8, left).

$$\begin{aligned} \dot{x} &= -\frac{\rho}{2}(\omega_R + \omega_L) \sin(\theta) \\ \dot{y} &= \frac{\rho}{2}(\omega_R + \omega_L) \cos(\theta) \\ \dot{\theta} &= \frac{\rho}{D}(\omega_R - \omega_L), \end{aligned}$$

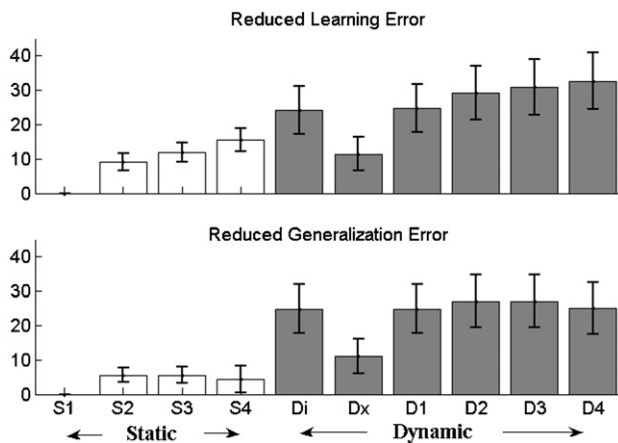


Figure 9. The reduced fitting (learning, upper plot) and testing (generalization, lower plot) errors with various neuronal models. The reduction factor is expressed as a change (in percent value) with respect to the errors of the linear static model (S1). The other bars stand for polynomial models up to fourth order (S2–S4), dynamic linear model (D1) and dynamic model with polynomial input function up to fourth order (D2–D4). Di stands for dynamic linear model without contralateral connections, and Dx stands for dynamic linear model without ipsilateral connections (see figure 7).

where (c_x, c_y) are the coordinates of the Khepera's center with respect to a fixed laboratory frame, θ is the angle of the line passing through the wheels (the axle) with respect to the x -axis of the same frame, ρ is the wheel radius (0.3 cm) and D is the axle length (5.3 cm). The state of this system is described by the vector (c_x, c_y, θ) . The input is the 2D vector, (ω_L, ω_R) , of angular velocities of the left and right wheels.

The light intensity observed by the sensors at the right and left sides of the robot (i_L, i_R) is inversely proportional to the square distance to the light source (see figure 8, right):

$$i_{R/L} = \frac{I}{r_{R/L}^2} \cos(\phi_{R/L}).$$

The angle ϕ is the 'preferred direction of the sensor', that is the direction of maximum response. The source is fixed in the environment and has an emission intensity, I . Under these assumptions, the intensity signals, (i_L, i_R) , are both functions of the robot's state: $i_{R/L} = i_{R/L}(c_x, c_y, \theta)$.

The loop was closed by means of the neural preparation that received stimulation proportional to the light intensity and generated neural activity that dictated the wheels velocity.

In our simulations the first-order dynamic system described above was controlled by the discrete neuronal models.

3.8. Recurrent dynamics

Figure 9 shows a summary of the results with the different models.

We found a greater error reduction with the dynamic models than with the static models, even when the latter include more parameters. The upper bar-plot in figure 9 shows the reduction in learning errors as a percentage of the learning error with the static linear (S1) model. It is obviously expected

that the error would be smaller with increasing complexity of the model. The Akaike information criterion suggests favoring the model that minimizes the following balance between the number of parameters (d) and the variance of the error (V) taking into account the number of data points (N): $\log(V) + 2d/N$. According to this tradeoff the best model is the dynamic linear model with only recurrent ipsilateral connections (figure 7(f)). This initial calculated guess is corroborated by careful analysis of the generalization data as well as physiological considerations as described below.

The lower bar-plot in figure 9 shows the reduction in generalization error, which is the error over data that were not used for the fitting. Note that the advantage of the dynamic model appears both in the learning and in the testing errors. A one-way analysis of variance (ANOVA) over the generalization errors of the eight models (S1–S4, and D1–D4) clearly rejects a null hypothesis that the models' mean errors are equal ($p < 0.01$). A Student's t -test shows that the mean error of the first-order dynamic model is significantly lower than the errors of the first two static models ($p < 0.01$). The first-order dynamic model reduced the error by 25%. In contrast, adding further complexity to the model led only to reducing the error by a few percentage points. The dynamic models, D2 or D3, generate the greatest reduction in generalization error. However, the difference between all dynamic models is statistically insignificant ($p > 0.01$). Non-parametric tests have provided similar results: a one-way non parametric analysis of variance (KRUSKALWALLIS ANOVA) over the generalization errors of the ten models (figure 9) clearly rejects a null hypothesis that the models' mean errors are equal ($p < 0.01$). Wilcoxon rank sum test for equal medians shows that the mean error of the first order dynamic model is significantly lower than the errors of all the static models ($p < 0.01$). The differences between D2, D3 or D4 and D1 are statistically insignificant ($p > 0.6$, Wilcoxon rank sum test for equal medians).

Since in this cross validation analysis we did not take into account the number of parameters, we used this consideration for choosing among the equally good models. Therefore, the first-order dynamic model (figure 7(c)) was selected for further analysis as a better candidate than any static model. One should keep in mind that this is an average over preparations and over trajectories to different light sources. As this average included many data points, it hides many details. Nevertheless, the advantage of the dynamic model, which contains just eight parameters, over any static model is apparent.

3.9. Neuroanatomical constraints and physiological basis for recurrence

The known anatomy of the lamprey nervous system does not support the presence of direct connections between reticular neurons across the midline. Therefore we may predict that a model with such contralateral connections would behave poorly. Accordingly, we have considered separately a model without recurrent contralateral connections (figure 7(f)), and a model without recurrent ipsilateral connections (figure 7(e)). The analysis clearly supports our expectations (see the two

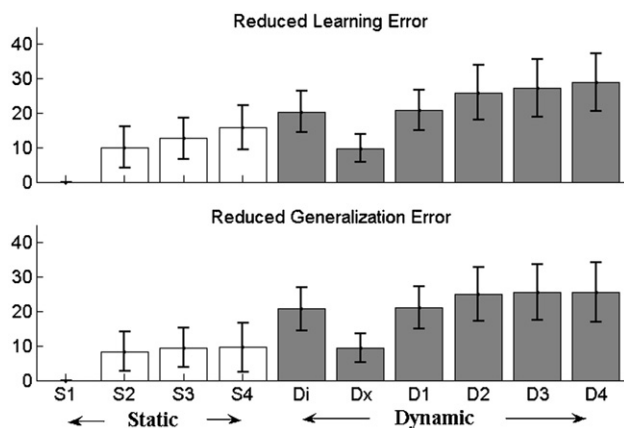


Figure 10. Reduced errors with various neuronal models in preparations where the spinal cord was transected. Note the similarity with figure 9, which reports preparations with intact spinal cord. See the caption of figure 9 for details.

middle bars in figure 9). Guided by Occam's razor principle among the equally effective models, we favor that with fewest parameters. This is the dynamic linear model with only recurrent ipsilateral connections, figure 7(f). Note that according to the Wilcoxon rank sum test this linear model with just six parameters outperformed all the static linear and nonlinear models ($p < 0.01$) and is not significantly different from all the nonlinear dynamic models ($p > 0.6$). We measured the performance by comparing the mean square error over the test data (the data that were not used for fitting).

The known anatomy suggests the presence of pathways from the brainstem to the spinal cord and back (see e.g., Grillner *et al* (2000)). This is one possible explanation for the improved fitting of models with recurrent connections. In order to test this hypothesis we have transected the spinal cord in four preparations and repeated the same protocol. These preparations generated similar results as the intact spinal cord. The learning and generalization were similar to figure 9, and in particular, the reduced error with the dynamic model was still about 25% (see figure 10). Therefore, we conclude that the recurrence afforded by bi-directional spinal cord pathways is not the likely reason for the dynamics expressed by the recurrent connections in the model. In the discussion section we suggest alternative accounts for the observed dynamic properties.

3.10. Dynamic properties and behavior

The taxonomy of behaviors for the static model was well studied (Braitenberg 1984, Fleming *et al* 2000). The possible behaviors include moving toward the light (positive phototaxis), away from the light (negative phototaxis) or circling the light (positive/negative menotaxis). In this study, the dynamic model added the possibility for instability and oscillations. Furthermore, the neural system is discrete. This generates a hybrid continuous–discrete system, which is not easily amenable to analytic insight.

In order to demonstrate the implications of the dynamic neural model on the possible behavior of the robot, we have

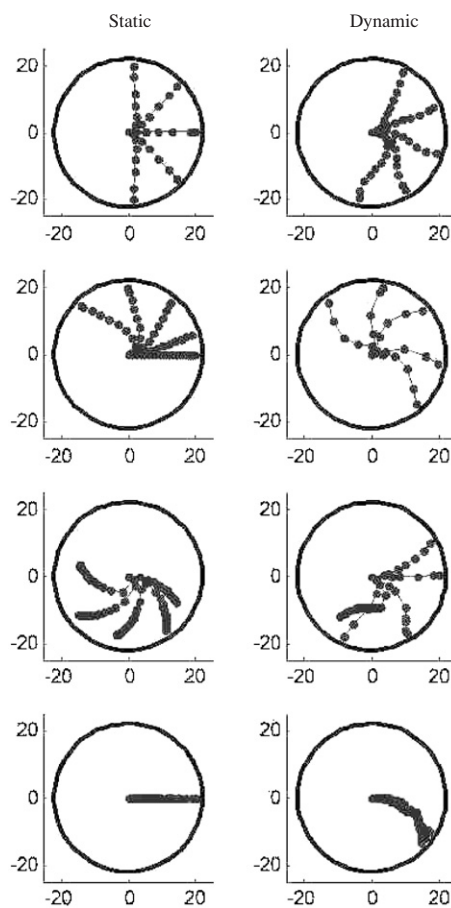


Figure 11. Simulation of robot behavior. Four examples with a static linear model (left) and four with a dynamic first-order model with only ipsilateral connections (right).

simulated the robot movements under the control of the static and the dynamic neural models (figure 11).

In this example, the static model was of the first order (figure 7(a)). The dynamic model was also of the first order and with only ipsilateral connections (figure 7(f)).

While all the tested models are capable of generating a broad repertoire of behaviors, there are two potentially important differences in the robot trajectories produced by static and dynamic models. (1) Models with recurrent dynamics tend to display more undulations in the trajectories than strictly static models. (2) Models with recurrent dynamics display crossover of trajectories. These two phenomena reflect the presence of second-order dynamics in the neuro-robotic system which introduces another state variable.

4. Experiment 2: induction and analysis of plastic changes

Following studies that demonstrated compensation in behaving lampreys after unilateral lesion of the vestibular capsules (Deliagina 1997), we tested the hypothesis that a plastic change in neural connections could be induced by the following protocol. First, we electronically 'blinded'

the left side of the robot by substantially reducing the gain of the light sensors on the left side of the robot from 1.0 to 0.1. This reduction was sufficient to suppress almost completely all stimulations to the left PRRN, thus simulating a unilateral labyrinthectomy. Next, the robot moved about the workspace for 20 min, either following a flashlight held by the experimenter or moving toward the workspace perimeter lights after starting from the center of the workspace. The purpose of this protocol was to establish an imbalance between the two input channels as the system was engaged in phototactic behavior and test whether this imbalance is sufficient to induce a long-lasting change in the input/output response of the neural population connected to the device. In carrying out the manual stimulation, care was taken to illuminate in similar amounts both the right and the left sensors. While the more automatic procedure offered a more controlled condition, the manual procedure had less pauses and allowed for more extensive stimulation in the same period of time. Nevertheless, both procedures resulted in the same macroscopic effect. Trajectory sets were measured (with the gain of the left light sensors at 1.0) for an hour before the plasticity protocol and for an hour afterward allowing a resting period of 5–10 min between trajectory sets. A critical feature of this procedure is that the measurements were carried out with the neuro-robotic system in the same normal condition. The artificial lesion was only applied during the training period. For a control experiment, we followed the same procedure except that the gain of the light sensors on the left side of the robot remained at 1.0 during the 20 min of random stimulation.

Figure 12 demonstrates the whole procedure from light intensity to stimulation and from recording to wheels velocity and trajectory of the movement for one preparation before and after the plasticity protocol.

The plasticity protocol succeeded in inducing an observable and statistically significant change in the robot's behavior. This was typically a change in the movement direction toward the right side of the workspace.

4.1. Tendency toward the right after the plasticity protocol

Figure 13 shows typical results of the plasticity protocol. This sample of four preparations demonstrates the wide variability as well as a tendency of the robot to turn to the right after a period of training with the left sensor occluded. Both sets of trajectories were obtained in identical conditions, with inputs from both right and left sensors.

The group analysis (figure 14) that compares the direction change after the plasticity protocol to the lack of change in a control group confirms these observations. However, one should note that the results are quite variable. As each preparation behaved differently the result reported here only reflects the net tendency to turn to the right.

4.2. Weights' change during adaptation

The change in direction after exposure to the artificial lesion can be accounted for by either a reduction in the spinning of the right wheel or by an increase in the spinning of the left wheel. Therefore, either a potentiation of the synapses on the left or

a depression of the synapses on the right (or a combination of both) could lead to the observed behavior.

To establish which neural change was actually responsible for the change in the robot's motion, we selected the preparations that resulted in a significant adaptive rotation to the right ($n = 9$) and fitted the first order dynamic model with recurrent ipsilateral connections (figure 7(f), six parameters). The values of these parameters before and after the plasticity protocol were compared and the difference is presented in figure 15. The reduction in the recurrent ipsilateral connection of the right side (V_{RR}) is consistent with the turn to the right. It is interesting that the most significant change occurred in the recurrent dynamic parameter. We interpret this as a general reduction in the responsiveness of the reticular neurons on the right side, induced by a period of reduced contralateral input from the left vestibular afferents. To confront this interpretation with direct observation of activity, we have calculated the autocorrelation of each output before and after the plasticity protocol (figure 16). This analysis shows a reduction in the autocorrelation of the right side, which is consistent with the change in the right dynamic weight in our simple model.

The physiological interpretation of this result must take into account that the connection between recording electrodes and robot wheel could either be direct (right–right/left–left) or reverse (right–left/left–right). In both cases, the finding implies a reduced excitability of the neurons that received excitatory inputs from the 'lesioned' site. In the direct mode, the predominant behavior was a positive phototaxis, consistent with a predominance of crossed excitatory connections. In this case, a tendency of the robot to veer to the right was associated with a decreased activity of neurons on the same side, which received excitatory inputs from the left (blinded) electrode. In the reverse mode, the same tendency of the robot was associated with a reduced activity of neurons on the left side. However, the reverse mode was chosen because of a predominant ipsilateral pattern of excitation, which would have caused positive phototaxis in the direct mode. Thus, again, the neurons with dominant excitatory connections to the blinded side showed decreased excitability after the lesion was removed.

5. Concluding remarks

Brain–machine interfaces are often investigated with an emphasis on the machine, as tools for helping the disabled. To develop these tools, we need to gain a deeper operational understanding of neural behavior. The term 'operational' is used here to distinguish the goal of understanding signal behavior from the goal of understanding the underlying cellular and molecular mechanisms.

We have discussed two sets of experiments in which the brainstem of a lamprey was placed in communication with artificial devices, both simulated and physical. The use of simulated devices in the first experiment allowed us to estimate the complexity of the neural dynamics, in terms of its state-space dimensionality. A useful characteristic of simulated devices, such as those used here, is

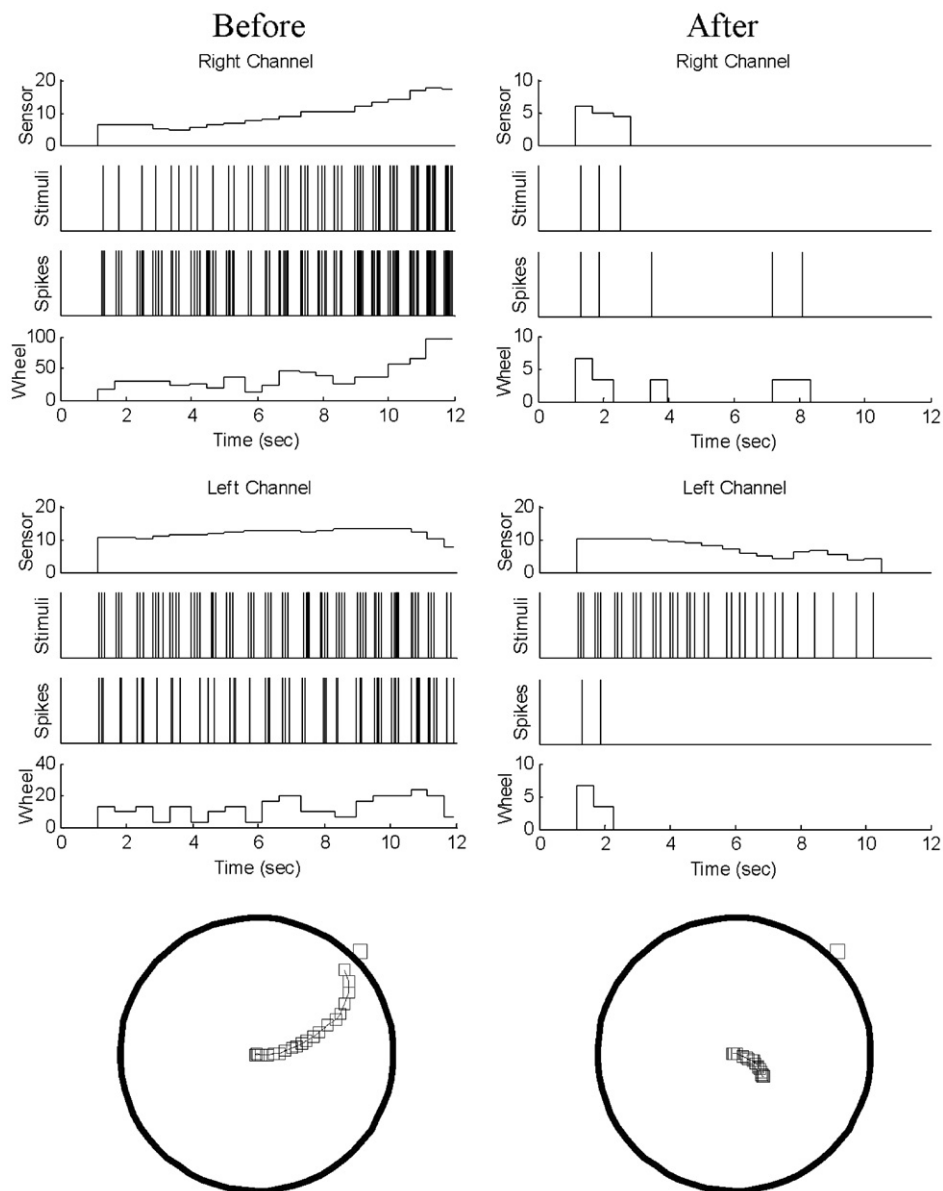


Figure 12. Hybrid system operation before (left) and after (right) the plasticity protocol. The workspace and the robot trajectories are illustrated in the bottom plate where the square at the periphery represents the location of the light that was turned on and stimulated the movement of the robot. The light intensity translated to spike rate (Hz) and to actual spikes to the same side of the preparation stimulated the neural tissue that generated the measured spikes translated to wheel velocity.

the possibility of establishing well-structured and arbitrary dynamical properties. This allowed us on one hand to design the simulated system so as to excite sufficiently broad dynamical ranges and on the other, to test the stability of the estimated neural dynamics by combining the neural tissue with artificial systems of different dimensions. The outcome of this first study is that the dynamical behavior is significant even in such a simple neural system, consisting of a single layer of neurons between stimulation and recording electrodes. However, the dimensionality that characterizes a single-input-single-output behavior is rather limited, the estimated range being between 2 and 4. We have used a well-established method for estimating the dimension of the neural system,

however one should note that there are other approaches to the same problem and, in particular, to the detection of chaotic dynamics amid noise (see, e.g., Barahona and Poon (1996) and Poon and Barahona (2001)). In particular, Poon and Barahona (2001) have developed a method for separating chaotic dynamics from noise, based on the gradual injection of (artificial) noise in increasing amounts on the data to be analyzed. We wish to stress that identification of a neural system's dynamics based on the two-way interaction with an external device can be carried out in combination with a variety of methods for the investigation of nonlinear dynamics, including but certainly not limited to the approach described here.

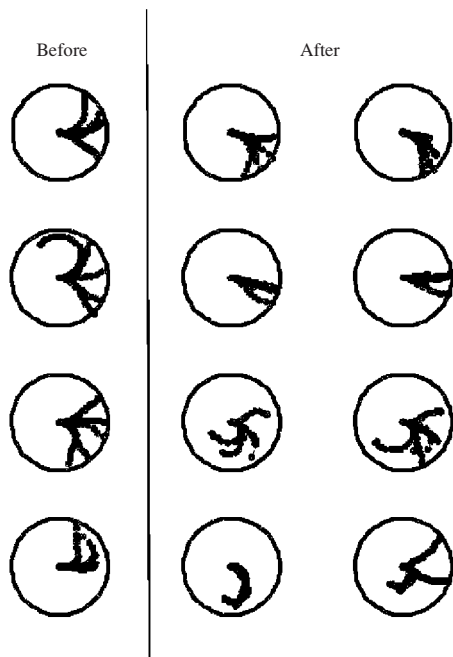


Figure 13. Typical trajectories of the robot before (left column) and after (two right columns) the plasticity protocol in four preparations. All sets of trajectories were obtained in identical conditions, with inputs from both right and left sensors. The middle column describes the first set of trajectories after the plasticity protocol and one can observe the tendency to move to the right. The right column is one of the last recorded trajectories (after about 10 min) where the effect of the adaptation is still apparent.

In the second experiment, we used a hybrid neuro-robotic system to study the properties of a neural population as it drives a two-wheeled robot. We have observed a tendency to change the behavior by moving to the right after a period of operation in which the left sensory input was selectively reduced. On the basis of combined observations of robot motions and of neural responses, we conclude that the best model of the operation performed by the neural element is a dynamic linear network with recurrent ipsilateral connections. We see two possible accounts for this result.

One account attributes the recurrent dynamics to an actual neural pathway. We considered the possibility for contralateral pathways and for pathways to the spinal cord and back. However, we found that a surgical transection of the spinal cord did not affect significantly the observed dynamical behavior.

A more likely interpretation suggests the presence of a local memory mechanism expressed by intrinsic neural properties (see e.g., Alford *et al* (1995), Schwartz and Alford (2000), Di Prisco *et al* (2000) and Kandel *et al* (2000)). This could be any mechanism, such as the threshold for plateau potentials, capable of establishing a relation between the tendency of a neuron to fire at one instant of time and the state of the neuron up to a few hundred milliseconds before. What is essential is that the neural activity does not depend exclusively upon the instantaneous synaptic input.

The neural pathways that we stimulated contained predominantly vestibular afferents, although cutaneous and visual pathways are also present. From an information

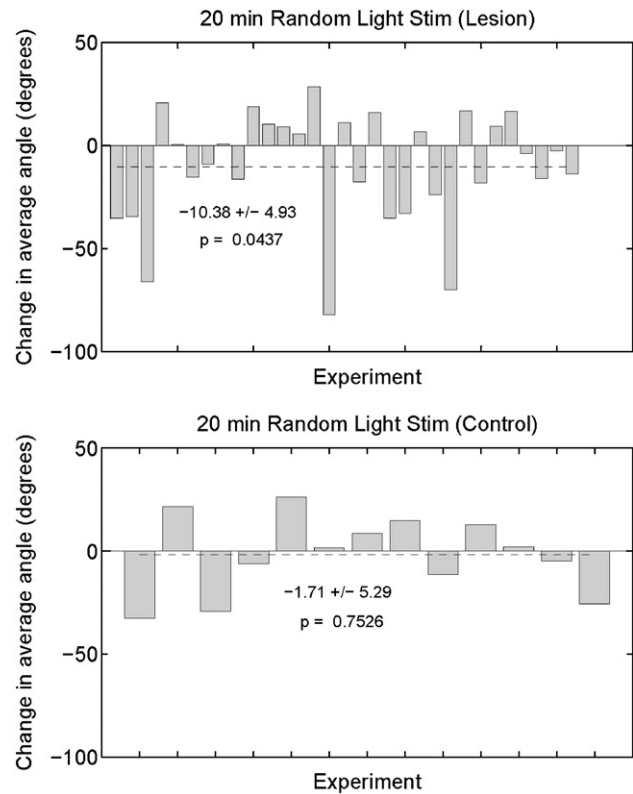


Figure 14. Average angle, after practice with the reversible lesion (upper plot), decreased by 10.38° ($p < 0.05$, $n = 31$). In the control case (lower plot), the average angle was not significantly different before and after the plasticity protocol ($p > 0.5$, $n = 13$). The average angle is calculated from the averaged velocity vectors in a single trajectory set (average of velocity vectors to all five lights). The velocity vectors were observed along the path described by the robot's movement to each single light (points closer than 0.5 cm are ignored because the robot could be relatively stationary at the beginning of a movement, creating a small, rotating vector).

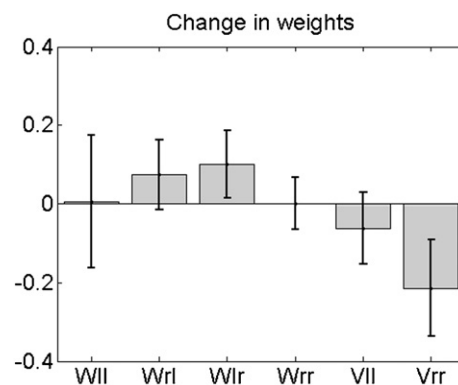


Figure 15. Change in the weights of the dynamic linear model without crossing connections (see figure 7(f)) before and after the plasticity protocol.

processing standpoint, there is a substantial degree of equivalence between the optical stimulation generated by the robot's sensors and the vestibular input. Both are right/left systems and a positive phototaxis corresponds to the tracking

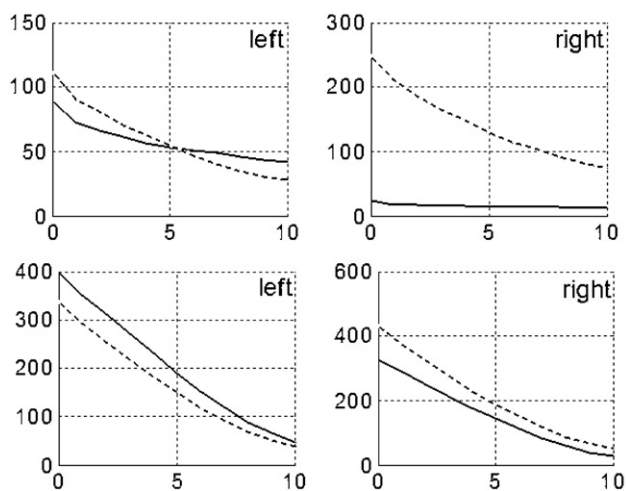


Figure 16. Autocorrelation of the neural activity before (dashed line) and after (solid line) the plasticity protocol. For one preparation (upper plate) and averaged over all preparations that demonstrated turn to the right (bottom). A decrease in the autocorrelation of the right side is observed after the plasticity protocol.

of a vertical direction. The semantics of the stimulus (gravity versus light) is not likely to play any substantial role here.

Hybrid neuro-robotic systems provide an artificial environment that is amenable to applying controllable and reversible perturbations for studying the operation of the nervous system. In the second experiment, we have introduced a ‘reversible artificial lesion’ by changing the output gain of light sensors. We saw this procedure as an alternative to irreversible surgical manipulations, such as the removal of a vestibular organ (unilateral labyrinthectomy). A clear advantage of the artificial lesion over the actual lesion is its complete reversibility. Another case for such neuro-robotic interfaces was presented by Zelenin *et al* (2000). In their study an electrical motor was used to rotate the lamprey and therefore provide feedback through the natural sensory system of the lamprey rather than through direct excitation, as in our study.

A significant feature of neuro-robotic interfaces is the control that they offer to the experimenter over the exact feedback that is provided through the artificial system and its sensors. By manipulating this feedback it is possible to study neural mechanisms, such as the dependence of plastic changes upon the correlation between presynaptic input and postsynaptic activity.

Investigation of the rules that govern synaptic plasticity in a hybrid system may lead to finding effective methods for ‘programming’ neural tissue so that it can execute a desired task. This goal is of central importance for the development of effective neural prostheses. Once a signal interaction is established between brain tissue and an external device, one can expect that the properties of the neurons interacting with the device will evolve on the basis of the history of signal exchange. Neural plasticity is perhaps the most important resource for establishing a working interaction between brain and external devices. Neuro-robotic interfaces provide a new

instrument for the direct investigation of how plasticity can be harnessed for generating desired behaviors.

Acknowledgments

This work has been supported by ONR grant #N00014-99-1-0881.

References

- Abarbanel H 1996 *Analysis of Observed Chaotic Data* (New York, NY: Springer)
- Alford S, Zompa I and Dubuc R 1995 Long-term potentiation of glutamatergic pathways in the lamprey brainstem *J. Neurosci.* **15** 7528–38
- Arnold V 1978 *Ordinary Differential Equations* (Cambridge, MA: MIT Press)
- Barahona M and Poon C-S 1996 Detection of nonlinear dynamics in short, noisy time series *Nature* **381** 215–7
- Bhushan N and Shadmehr R 1999 Computational nature of human adaptive control during learning of reaching movements in force fields *Biol. Cybern.* **81** 39–60
- Braitenberg V 1984 *Vehicles—Experiments in Synthetic Psychology* (Cambridge, MA: MIT Press)
- Carmena J M, Lebedev M A, Crist R E, O’Doherty J E, Santucci D M, Dimitrov D F, Patil P G, Henriquez C S and Nicolelis M A L 2003 Learning to control a brain-machine interface for reaching and grasping by primates *PLoS Biol.* **1** 193–208
- Deliaquina T G 1997 Vestibular compensation in lampreys: impairment and recovery of equilibrium control during locomotion *J. Exp. Biol.* **200** 1459–71
- Di Prisco G V, Pearlstein E, Ray D L, Robitaille R and Dubuc R 2000 A cellular mechanism for the transformation of a sensory input into a motor command *J. Neurosci.* **20** 8169–78
- Donoghue J P 2002 Connecting cortex to machines: recent advances in brain interfaces *Nat. Neurosci.* **5** 1085–8
- Fleming K M, Reger B D, Sanguineti V, Alford S and Mussa-Ivaldi F A 2000 Connecting brains to robots: an artificial animal for the study of learning in vertebrate nervous system *Proc. 6th Int. Conf. on Simulation of Adaptive Systems* (Cambridge, MA: MIT Press)
- Gottlieb G L 1994 The generation of the efferent command and the importance of joint compliance in fast elbow movements *Exp. Brain Res.* **97** 545–50
- Grillner S, Cangiano L, Hu G-Y, Thompson R, Hill R and Wallén P 2000 The intrinsic function of a motor system—from ion channels to networks and behavior *Brain Res.* **886** 224–36
- Haykin S 1999 *Neural Networks: A Comprehensive Foundation* 2nd edn (Englewood Cliffs, NJ: Prentice-Hall)
- Helms Tillery S I, Lin W S and Schwartz A B 2001 Training non-human primates to use a neuroprosthetic device *Society for Neurosciences Abstracts* 63.4
- Inbar G F and Yafe A 1976 Parameter and signal adaptation in the stretch reflex loop *Prog. Brain Res* ed S Homma (Amsterdam: Elsevier) pp 317–37
- Kandel E R, Schwartz J H and Jessell T M (ed) 2000 *Principles of Neural Science* 4th edn (New York: McGraw-Hill)
- Kaplan D T 1993 A model-independent technique for determining the embedding dimension *Chaos in Communications SPIE* vol 2038 ed L M Pecora pp 236–40
- Kaplan D T 1994 Exceptional events as evidence for determinism *Physica D* **73** 38–48
- Kaplan D T and Glass L 1992 Direct test for determinism in a time series *Phys. Rev. Lett.* **68** 427–30

- Karniel A and Inbar G F 2000 Human motor control: learning to control a time-varying non-linear many-to-one system *IEEE Trans. Syst., Man Cybern. C* **30** 1–11
- Kawato M 1999 Internal models for motor control and trajectory planning *Curr. Opin. Neurobiol.* **9** 718–27
- Kennel M B, Brown R and Abarbanel H D 1992 Determining minimum embedding dimension using a geometrical construction *Phys. Rev. A* **45** 3403–11
- Kositsky M, Karniel A, Alford S T, Fleming K M and Mussa-Ivaldi F A 2003a Dynamical dimension of a hybrid neuro-robotic system *IEEE Trans. Neural Syst. Rehabil. Eng.* **11** 155–9
- Kositsky M, Chiappalone M, Acosta S and Mussa-Ivaldi F A 2003b Identification of neural dynamics by interfacing with artificial devices *33rd Annual Meeting of Society for Neuroscience (New Orleans, LA)*
- Mane R 1981 On the dimension of the compact invariant sets of certain nonlinear maps *Dynamical Systems and Turbulence, Warwick 1980* ed D Rand and L S Young (Berlin: Springer) p 230
- Musallam S, Corneil B D, Greger B, Scherberger H and Andersen R A 2004 Cognitive control signals for neural prosthetics *Science* **305** 258–62
- Mussa-Ivaldi F A and Bizzi E 2000 Motor learning through the combination of primitives *Phil. Trans. R. Soc. B* **355** 1755–69
- Mussa-Ivaldi F A and Miller L E 2003 Brain–machine interfaces: computational demands and clinical needs meet basic neuroscience *Trends Neurosci.* **26** 329–34
- Poon C-S and Barahona M 2001 Titration of chaos with added noise *Proc. Natl Acad. Sci.* **98** 7107–12
- Rovainen C M 1979 Electrophysiology of vestibulospinal and vestibuloreticulospinal systems in lampreys *J. Neurophysiol.* **42** 745–66
- Ruelle D 1990 Deterministic chaos: the science and the fiction *Proc. R. Soc. A* **427** 241–8
- Serruya M D, Hatsopoulos N G, Paninski L, Fellows M R and Donoghue J P 2002 Brain–machine interface: instant neural control of a movement signal *Nature* **416** 141–2
- Schwartz N and Alford S 2000 Physiological activation of presynaptic metabotropic glutamate receptors increases intracellular calcium and glutamate release *J. Neurophysiol.* **84** 415–27
- Shadmehr R and Mussa-Ivaldi F A 1994 Adaptive representation of dynamics during learning of a motor task *J. Neurosci.* **14** 3208–24
- Takens F 1981 Detecting strange attractors in turbulence *Dynamical Systems and Turbulence, Warwick 1980* vol 898 ed D Rand and L S Young (Berlin: Springer) p 366
- Taylor D M, Tillery S I H and Schwartz A B 2002 Direct cortical control of 3D neuroprosthetic devices *Science* **296** 1829–32
- Wessberg J, Stambaugh C R, Kralik J D, Beck P D, Laubach M, Chapin J K, Kim J, Biggs S J, Srinivasan M A and Nicolelis M A L 2000 Real-time prediction of hand trajectory by ensembles of cortical neurons in primates *Nature* **408** 361–5
- Wolpert D M, Ghahramani Z and Jordan M I 1995 An internal model for sensorimotor integration *Science* **269** 1880–2
- Zelenin P V, Deliagina T G, Grillner S and Orlovsky G N 2000 Postural control in the lamprey: a study with a neuro-mechanical model *J. Neurophysiol.* **84** 2880–7